Results in Optics 12 (2023) 100462

Contents lists available at ScienceDirect

Results in Optics

journal homepage: www.sciencedirect.com/journal/results-in-optics

Nonlinear optical properties of gold nanoparticles produced by laser ablation at two different radiation wavelengths

Bita Azemoodeh Afshar, Akbar Jafari *, Mir Maqsood Golzan, Rahim Naderali

Physics Department, Faculty of Sciences, Urmia University, Urmia, Iran

ARTICLE INFO

Keyword:
Size of gold nanoparticles
Laser ablation
Nonlinear Optical properties
Z-scan method

ABSTRACT

In this study, gold nanoparticles were synthesized by laser ablation of Au bulk in distilled water. The laser used is Nd: YAG laser, which has a fundamental harmonic wavelength ($\lambda = 1064nm$) and second harmonic wavelength ($\lambda = 532nm$). In order to control the size of Au nanoparticles (NPs), we used sodium citrate as a stabilizer. Morphology, structure and linear optical properties of Au NPs samples were characterized by transmission electron microscopy (TEM observation), XRD diffraction (XRD) and UV–Visible spectroscopy. Furthermore, the chemical structure in solution of Au NPs was studied by Fourier transform-infrared spectroscopy (FTIR). The nonlinear optical parameters of these Au NPs were studied using the Z-scan method. We found the optimal values of fluencies and laser pulse repetition rates to achieve the smallest size values and the most distribution of the produced gold nanoparticles. It is resulted that due to the very small size of NPs, the nonlinear optical parameters show larger values. It is 10^7 order of magnitude larger than what has been reported for the nonlinear refractive index in previous researches. In addition, gold nanoparticles that are produced with a laser wavelength of 1064 nm and have a high nonlinear refractive index can be used in chip-based sensors. Finally, the use of these Au NPs in optical switching devices was investigated by the two figures of merit method, which indicated that these Au NPs are practical tools for optical switching devices.

1. Introduction

Gold nanoparticles (Au NPs) have more applications in electronics (Hajiesmaeilbaigi et al., 2006; Nastulyavichus et al., 2018), biosensors (Kong et al., 2004; Saha et al., 2012); biological imaging, and nanomedicine domain (Cai et al., 2008) due to their chemical stability and unique optical properties. Their surface-Plasmon resonance (SPR) is located in the visible region (Sadrolhosseini et al., 2014). The refractive index sensing property of Au NPs is used in the constructing of SPR-based refractometric sensors (Sadrolhosseini et al., 2017). Surface-Plasmon properties of Au NPs make them usable in Plasmon sensors (Sadrolhosseini et al., 2014; Sadrolhosseini et al., 2017). The response of Au NPs to an interaction of light beam has been dependent on their size, shape, concentration, and the surrounding medium. Depending on their shape and structure, Au NPs have important optical properties used in spectroscopic detection and photothermal therapy (Gentile et al., 2021). On the other hand, some antibacterial, optical, and catalytic properties of Au NPs increase for particle sizes smaller than 15 nm (Svedendahl et al., 2009). Many methods are used in the formation of Au NPs, such as chemical methods (Huang and El-Sayed, 2010; Calderen-Jimenez and Montoro Bustos, 2022), microwave method (Faraday, 1857), sono-chemical method (Turkevich et al., 1951), and laser ablation (Das et al., 2012; Okitsu et al., 2005). Laser ablation is the fastest and safest method to produce colloidal NPs in a liquid environment, which strongly changes the surface chemistry, and physical properties. In laser ablation, the laser beam hits the metal surface and some of the incident pulse energy is absorbed by the metal and turns into heat. The metal starts to melt in that part. As the temperature increases, the metal melts and begins to vaporize, and the resulting vapor covers the surface of the metal. Part of the energy of the beam is absorbed by the resulting vapor, as the temperature rises, the vapor pressure on the metal increases. A further increase in temperature causes the vapor to ionize and a part of vapor turns into plasma. The cloud-like column of vapor and plasma created is called plasma smoke. Plasma smoke consists of atoms, ions and molecules of ablation substances, which spread in the liquid environment along with the propagation of shock waves, and during the expansion process, the plasma smoke cools down and gives its energy to the liquid environment, this phenomenon leads to the formation of

* Corresponding author.
E-mail address: a.jafari@urmia.ac.ir (A. Jafari).

https://doi.org/10.1016/j.rio.2023.100462
Received 23 April 2023; Received in revised form 30 May 2023; Accepted 26 June 2023
Available online 30 June 2023

bubbles. The created bubble collapses with the release of the second shock wave. This action is repeated during the ablation time. The particles created in the liquid medium are dispersed and the corresponding metal NPs are generated as the most likely product. Laser ablation of solids in liquid environments is an alternative method compared to other methods of NPs synthesis due to its simple experimental setup. The approach allows the growth of metal NPs in a controlled environment, which is a crucial step for a successful surface functionalization of metal NPs (Das et al., 2012; Okitsu et al., 2005). In laser ablation, there is no reduction of a chemical agent or toxicity surfactants used. As a result, the laser ablation method keeps and preserves the gold nanoparticle purity, quality and homogeneity (Atile et al., 1987; Pyatenko et al., 2004; Jiménez et al., 2010). Ying et al., n.d. reported Ag NPs which were produced under Focused nanosecond IR laser pulses ($\lambda = 1064$ nm) in air without stabilizers. The size of NPs and linear absorption spectrum of NPs were studied (Nastulyavichus et al., 2018). (Sadrolhosseini et al., 2014) reported the synthesis of Au NPs by second harmonic Q-switched Nd:YAG laser without stabilizers in the graphene oxide gel. The optical properties of Au NPs were studied per one laser fluency and different laser ablation times and different concentrations of the Go gel. The obtained average diameters of NPs were at the range of 5.18–16.55 nm (Sadrolhosseini et al., 2014). The effect of temperature on the Au NPs size per one laser fluency, per one pulse repetition rate and different laser ablation times was studied by (Sadrolhosseini et al., 2017). The obtained average diameters of NPs with spherical shape were at the range of 8.92–19.93 nm (Sadrolhosseini et al., 2017). The solution structure of gold nanoparticles was investigated using small-angle X-ray scattering (SAXS) by L. (Gentile et al., 2021). The analysis of the SAXS curve shows the presence of a large number of small aggregates with a fractal structure. The fractal dimension of Au NPs was d = 1.9 nm (Gentile et al., 2021). The Au NPs were formed in tetrahydrofuran, nonorganic liquid and graphene oxide using laser ablation without stabilizers (Weber et al., 1978). The researches that have been reported so far for the production of NPs by laser ablation, have been using one laser fluency, one number of the laser pulses and one radiation wavelength at different times without adding a stabilizer. So that the average size of NPs has large values. In this work, the stabilizer acts like a soft template and keeps the NPs apart and prevents the NPs from merging. As a result, the size of NPs becomes smaller. In two different wavelengths, by changing the laser fluency and laser pulse repetition rate, the best mode for producing gold nanoparticles with very small dimensions has been obtained. For the production of NPs with dimensions of 1.93 nm and 8.82 nm at the laser pulse repetition rate of 12 *Hz*, the best laser fluencies were obtained 0.017 J/cm^2 for $\lambda = 532nm$ and 0.028 J/cm^2 for $\lambda = 1064nm$, respectively. Since the average size of NPs shows small values, the nonlinear parameters show larger values (it is 10^7 order of magnitude larger than what has been reported for the nonlinear refractive index in previous researches) than those previously reported in articles (Sadrolhosseini et al., 2014; Huang and El-Sayed, 2010; González-Castillo et al., 2017; Shahriari et al., 2010; MatIsa and Zainon, 2022).

Obtaining highly stable Au NPs smaller than 15 nm in a controlled environment has attracted significant interest from the scientific community (Jiang et al., 2022). In recent years, Vinceunas et al. (Sadrolhosseini et al., 2014; Maciulevičius et al., 2013) produced Au NPs by laser ablation without stabilizers. The Nd: YAG laser with $\lambda = 532nm$ was used for the ablation process. The average diameter of NPs with the shape of spherical was 27.5 nm. Saitow et al. (Saitow et al., 2012; Jiang et al., 2022) produced Au NPs by laser ablation with an ns-pulsed laser. The average diameter of NPs with the shape of fractal structure was 20 nm. R. Zainon et al (MatIsa and Zainon, 2022) produced Au NPs by laser ablation without stabilizers. The Nd: YAG laser with $\lambda = 1064nm$ was used for the ablation process. The average diameter of NPs with the shape of spherical for $\lambda = 1064nm$ was 12.09 nm. In this work, we produced the smaller Au NPs with a stabilizer for controlling the size of Au NPs and preventing the aggregation of NPs. The obtained average diameters of NPs with the shape of spherical are 1.93 nm produced by Nd:YAG laser at laser ablation wavelength $\lambda = 532nm$ and 8.82 nm at laser ablation wavelength $\lambda = 1064nm$.

There are many methods for analyzing the nonlinear optical parameters, such as nonlinear interferometry (Maciulevičius et al., 2013), degenerate four-wave mixing (Friberg and Smith, 1987), nearly degenerate three-wave mixing (Adair et al., 1987), and Z-scan. The Z-scan is a unique method used to measure the nonlinear refractive index and nonlinear absorption coefficient of NPs, which is the simplest method to evaluate the sign and amount of nonlinear optical parameters of NPs (Sheik-Bahae et al., 1990). Various studies have displayed the result of Z-scan measurements by the thermal concave (convex) lens in the medium around the metal NPs due to the tangible heat transfer from the metal NPs to the medium or by the difference between the refractive index of metal NPs and the medium (Tan and Omar, 2019).

Moreover, Agents affect the type and size of Au NPs and can protect the NP core from aggregation. In addition, the agents can improve the stability related to the lifetime of NPs used for different applications (González-Castillo et al., 2017). In recent years, for example, De Goes et al. (De Góes et al., 2017; Góes et al., 2020) used sodium citrate as a stabilizer, and capping Ag NPs in water solution to detect the amount of glyphosate in water by laser ablation method. Ruffino et al. (Sortino et al., 2020) used sodium citrate as a stabilizer, and capping Au NPs in water solution to detect the amount of glyphosate in water by laser ablation method. Glyphosate is used to control weeds and vegetation in gardens and an increase the amount of glyphosate poses a risk to human health.

In this work, we report the synthesis of gold NPs with an average size smaller than 15 nm by laser ablation in distilled water. We also used 1 mg of sodium citrate for stabilization purposes (sodium citrate is used as a stabilizer to prevent Au NPs aggregation). We investigated the effect of laser fluency and laser ablation wavelengths on the size of gold NPs and the nonlinear properties of gold NPs. The size of NPs can be controlled by increasing or decreasing the laser fluency and the wavelength of the laser radiation. Finally, the main aim of this work is described as: in two different wavelengths, by adding a stabilizer and changing the laser fluency and laser pulse repetition rate, the best mode is obtained for the production of gold nanoparticles with very small dimensions to achieve high values of nonlinear optical parameters. The samples were characterized by linear absorption spectroscopy and transmission electron microscopy. The nonlinear properties of Au NPs including nonlinear refractive and nonlinear absorption coefficient were studied. The theoretical analysis based on Sheik-Bahaee model is in agreement with the experimental results of the Z-scan method for Au NPs in water. Samples produced with extended laser ablation wavelengths exhibit a broad nonlinear refractive index, which can be used to develop nanoplasmonic sensing platforms. This study gives a broad outline for selecting Au NPs for improving chip-based sensor systems. Finally, two figures of merit ($|w| \gg 1$ and $|T| \ll 1$) were gained to evaluate the applications of Au NPs in all-optical switching devices (Fan et al., 2009).

2. Experiment

2.1. Laser ablation for producing Au nanoparticles

The laser ablation setup contains a lens, and an ns-pulsed laser. In this work, we used Q-switched Nd: YAG laser and a liquid container (a Teflon vessel). The gold target (99.9%) is submersed in distilled water and 1 mg of Sodium citrate (Sodium citrate acts as a soft template to keeps apart and prevents the NPs from aggregating). Fig. 1 shows the laser ablation setup, which contains a Q-switched Nd:YAG laser (with a pulse repetition rate with frequencies of 0–22 *Hz*), a gold plate, and a lens ($f = 5$ cm). The surface of the gold target is 1 cm^2, the volume of distilled water is 2.8 cc, and a Teflon vessel with a diameter of 1.6 cm. An open-air condition and a pulse repetition rate with the frequency of 12 *Hz* were used to prepare Au NPs. In order to achieve the smallest size

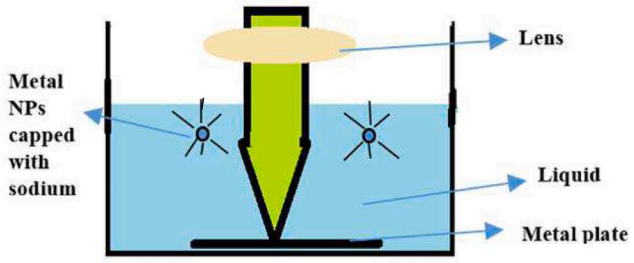

Fig. 1. The experimental arrangement for producing Au NPs by laser ablation.

and the most distribution of gold nanoparticles, we found the optimal laser intensity value for each laser wavelength the best laser fluencies at the laser pulse repetition rate of 12 *Hz*, were obtained 0.017 J/cm^2 for $\lambda = 532nm$ and 0.028 J/cm^2 for $\lambda = 1064nm$, respectively. The duration of pulse for the fundamental line ($\lambda = 1064nm$) of a Q-switched Nd:YAG laser was five ns, and for its second harmonic line ($\lambda = 532nm$), was 4 ns. The laser ablation time is 5 min.

2.2. Characterization of nanoparticles

After each ablation, 2.8 cc of the nanoparticle solution was put into a quartz cell with a width of 1 cm for the UV–Visible optical spectral characterization. The UV–visible spectrum of samples was recorded with a HALO XB-10 spectrophotometer.

Morphology (the particle size and size distribution) of the prepared samples was obtained with the TEM (CM120, the Netherlands) method. For TEM measurements, a drop of the solution containing Au NPs was deposited and dried on a carbon-coated copper grid.

2.3. Z-scan setup

Nonlinear properties of Au NPs, such as nonlinear absorption coefficient and nonlinear refractive index, were measured using the Z-scan method. The setup of the Z-scan is displayed in Fig. 2.

The Z-scan setup consists of the second harmonic of a continuous wave diode-pumped Nd:YAG laser with $\lambda = 532nm$ and an output power of 64 mW, pinhole, and lens (f=10 cm), travel linear stage (z-axis), quartz cell with a width of 2 mm and two photodiodes. The TEM00 mode of the laser beam was Focused by a lens with a focal length of f=10 cm. The cell was moved along Z-axis (−50 mm–+50 mm), and the nonlinear optical data of refractive index and absorption coefficient were recorded by two photodiodes, PD_1 and PD_2, respectively.

2.4. Fourier transform-infrared spectroscopy (FTIR)

Fourier transform-infrared spectroscopy (FTIR) is a powerful tool for chemical and biochemical studies, which is used in the detection of various functional groups.

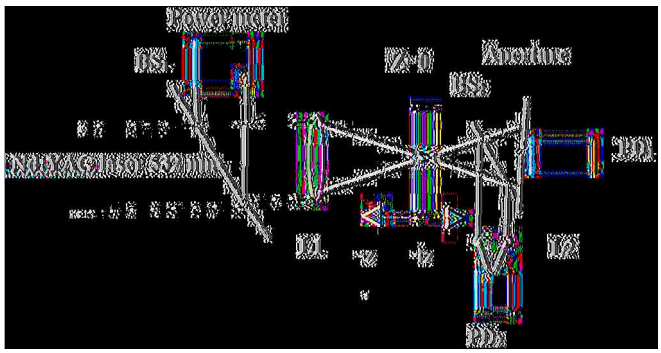

Fig. 2. Arrangement of Z-scan method.

2.5. X-ray powder diffraction pattern (XRD)

X-ray powder diffraction pattern is used to determine the crystal structure of gold nanoparticles.

2.6. Two figures of merit

The Au NPs suitable candidates for optical switching devices due to the presence of delocalized $\pi - electron$ s, and the transforming electron densities between the Au NPs, and ligands. For the application of Au NPs in all-optical switching devices, we used the following two figures of merit (Fan et al., 2009):

$$W = \frac{n_2 I_0}{\alpha_0 \lambda}, \tag{1}$$

And

$$T = \frac{\beta \lambda}{n_2}, \tag{2}$$

In which I_0 is the laser intensity at the focus of the converging lens and λ is the wavelength at Z-scan. For the suitability of these NPs in all-optical devices, it is necessary to obtain $|W| \gg 1$ and $|T| \ll 1$([28]).

3. Discussions and result

3.1. Au nanoparticles characterization

Fig. 3 shows the UV–visible spectrum of nanoparticle solution prepared by ablating an Au target in 2.8 cc distilled water and 1 mg of Sodium citrate through focusing laser light at two different laser ablation wavelengths ($\lambda = 532nm$ and $\lambda = 1064nm$). The spot size was 1 mm. The optimum time for ablation was 5 min and there is no absorption peak less than 5 min. Sodium citrate was used as a stabilizer to control the size of Au NPs (Sivakumar et al., 2011). The interaction between Sodium citrate and Au^+ was strong (interaction between Au^+ ions and COO^- group in Sodium citrate formula and OH group in water). The aqueous solution contained Au^+ ions, COO^-, and OH groups. Gold NPs vapor or gold plasma was produced by laser ablation. During ablation, Sodium citrate and water started to decompose by ablating laser, and Sodium citrate caps Au^0 and Au^+ ions. Different laser fluencies at each constant pulse repetition rate at two different laser ablation wavelengths were tested in laser ablation to produce Au NPs from 0.0069 J/cm^2 to 0.127 J/cm^2. Furthermore, Au NPs were not produced for constant laser fluency and varying pulse repetition rates. Thus, for a pulse repetition rate of 12 *Hz*, and two different laser ablation wavelengths $\lambda = 532nm$ and $\lambda = 1064nm$, the optimal laser fluencies for the production of Au NPs were 0.017 J/cm^2 and 0.028 J/cm^2, respectively.

The linear absorption coefficients were obtained through the following equation (Rad et al., 2012):

$$\alpha_0 = -\frac{1}{L} LnT, \tag{3}$$

Where L = 1 cm is the cell thickness, and T is the light transmission. Fig. 3 shows the process of finding the optimum laser fluency to produce Au NPs.

According to Fig. 3(a), the UV–visible peaks for the 12 *Hz* pulse repetition rate in the laser radiation wavelength, 532 nm, at three different laser fluencies: 0.024 J/cm^2 and 0.017 J/cm^2, and 0.007 J/cm^2 appeared at about λ = 443 nm and λ = 473 nm and λ = 460 nm, respectively. Since the surface Plasmon resonance occurred at shorter wavelengths for large Au NPs, the size of Au NPs at 0.017 J/cm^2 is the smallest of the three laser fluencies. As a result, the optimum laser fluency to produce Au NPs at the pulse repetition rate of 12 *Hz* and the laser radiation wavelength of 532 nm was 0.017 J/cm^2.

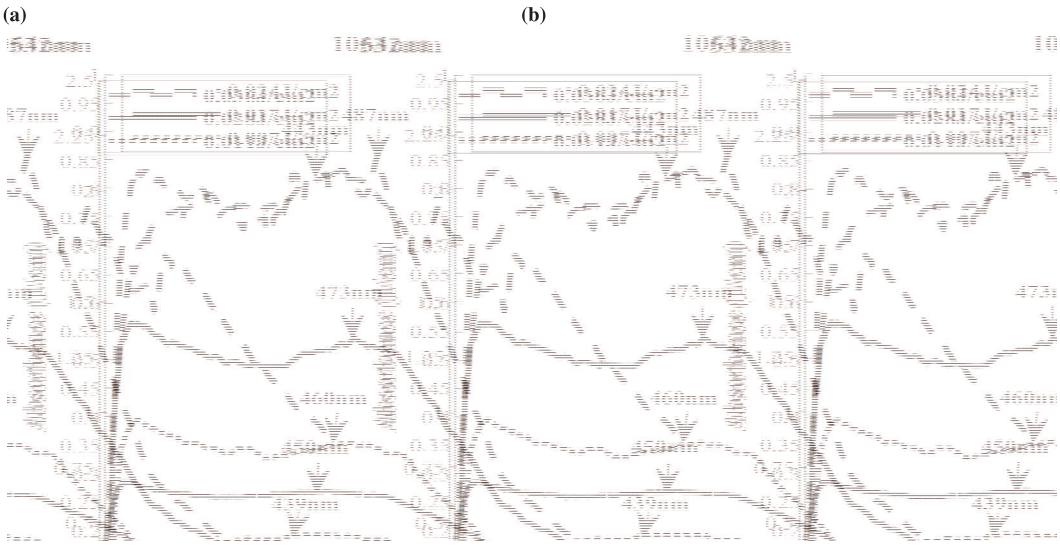

Fig. 3. UV–visible spectrum of Au NPs at the pulse laser repetition rate with 12 *Hz* in (**a**) the laser radiation wavelength 532 nm and three different laser fluencies: 0.024 J/cm^2 and 0.017 J/cm^2, and 0.007 J/cm^2;(**b**) the laser radiation wavelength 1064 nm and three different laser fluencies: 0.036 J/cm^2 and 0.028 J/cm^2, and 0.011 J/cm^2.

According to the description of Fig. 3(a), the UV–visible peaks in Fig. 3(b) for the 12 *Hz* repetition rate in the laser radiation wavelength, 1064 nm, at three different laser fluencies: 0.036 J/cm^2 and 0.028 J/cm^2, and 0.011 J/cm^2 appeared at about $\lambda = 487$ nm and $\lambda = 450$ nm and $\lambda = 439$ nm, respectively. Since several peaks are seen in the UV–visible spectrum of laser fluency of 0.036 J/cm^2, so Au NPs are not formed in this laser fluency. As a result, the optimum laser fluency to produce Au NPs at a pulse repetition rate of 12 *Hz* and the laser radiation wavelength of 1064 nm was 0.028 J/cm^2 (Koebel et al., 2008; Mashayekh and Dorranian, 2017).

Since the surface Plasmon, resonance at the laser ablation wavelength 1064 nm occurred at a shorter wavelength than the laser ablation wavelength 532 nm, so the size of Au NPs at the laser ablation wavelength 1064 nm is large. On the other hand, the increasing the absorption peak intensity can be related to increasing the concentration of Au NPs in the solution, which, as indicated, the concentration of Au NPs at 0.028 J/cm^2 is higher than 0.017 J/cm^2. More absorption in a sample under irradiation with a larger laser ablation wavelength is due to the increase in the number of NPs in that sample. On the other hand, at large laser ablation wavelength ($\lambda = 1064nm$) and low laser fluency, self-absorption of radiation by solvent or metal NPs in the path of the radiant laser beam was low. As a result, increasing the wavelength of laser radiation can be related to increasing the concentration of Au NPs in the sample (Tan and Omar, 2019; Koebel et al., 2008; Mashayekh and Dorranian, 2017).

Fig. 4(a) and (c) demonstrate TEM images of Au NPs produced at two laser ablation wavelengths, 532 nm (with optimum laser fluency of 0.017 J/cm^2) and 1064 nm (with optimum laser fluency of 0.028 J/cm^2).

According to Fig. 4(b) and (d), the average size of Au NPs at the pulse laser repetition rate with 12 *Hz* in the laser fluency, F = 0.017 J/cm^2, and the laser ablation wavelength, 532 nm, for 27 number of Au NPs is 1.93 nm. For the laser fluency, F = 0.028 J/cm^2, and the laser ablation wavelength, 1064 nm, for 27 of Au NPs is 8.82 nm.

As can be seen from Fig. 4(a) and (c), the Au NPs are almost spherical in two samples, and the laser ablation wavelength does not affect the shape of Au NPs. Moreover, the size and size distribution have depended on the laser ablation wavelength and the laser fluency, which are in good agreement with Refs. (Tan and Omar, 2019) and (Mashayekh and Dorranian, 2017).

By comparing Fig. 4(b) and (d), we found that the average size of Au NPs in the laser ablation wavelength 532 nm is smaller than that of Au NPs in the laser ablation wavelength 1064 nm.

Furthermore, the distribution of Au NPs in the ablation wavelength 1064 nm is more than that of Au NPs in the laser ablation wavelength 532 nm.

As a result, the increase in the average size of Au NPs can be related to the increase in the wavelength of the ablation laser. This means that due to low self-absorption, larger NPs are produced with increasing laser wavelength at low laser fluencies. This is in agreement with the observation of the UV–visible spectrum at Fig. 3(a), (b).

As a result, the average size of NPs shows small values compared to what was reported in previous articles (Saitow et al., 2012; Jiang et al., 2022).

3.2. Nonlinear optical properties

3.2.1. Nonlinear refractive index measurements (closed aperture Z-scan method)

In the z-scan method, the sample was moved by a stepper motor along the z-axis with a step size of 0.1 mm. The laser intensity at the focus of the converging lens at Z-scan method, I_0, is 8.15 $\frac{W}{cm^2}$.

When a high irradiance of a laser beam passed through a nonlinear material, according to the dependence of refractive index on the radiation,$n = n_0 + n_2 I$, the case of $n_2 > 0 or n_2 < 0$ results in the self-focusing or self-defocusing phenomena, respectively(Jafari et al., 2018).

When the sample approaches the beam focus, irradiance increases, which leads to self-lensing in the sample, in the before of focal point of the lens, the sample acts as a negative (positive) lens, which leads to converging (diverge) the beam on the aperture (PD_1 in Fig. 2) in the far field, so the measured transmittance increases (decreases), respectively. In the after of the focal point of the lens, the inverse effect occurs (Mashayekh and Dorranian, 2017).

Theoretical data were obtained using the Sheik-Bahaee model for nonlinear optical parameters (Sheik-Bahae et al., 1990). In addition to the contribution of the data related to the nonlinear refractive index, the data related to the nonlinear absorption coefficient are also involved in PD_1. To eliminate the nonlinear absorption coefficient effect, the data of detector PD_1 were divided by the data of detector PD_2 by point by-point. Then, all the new data were normalized to the transmittance of the close aperture when no sample was present. The normalized peak to valley transmittance for close aperture is given as (Sheik-Bahae et al., 1990):

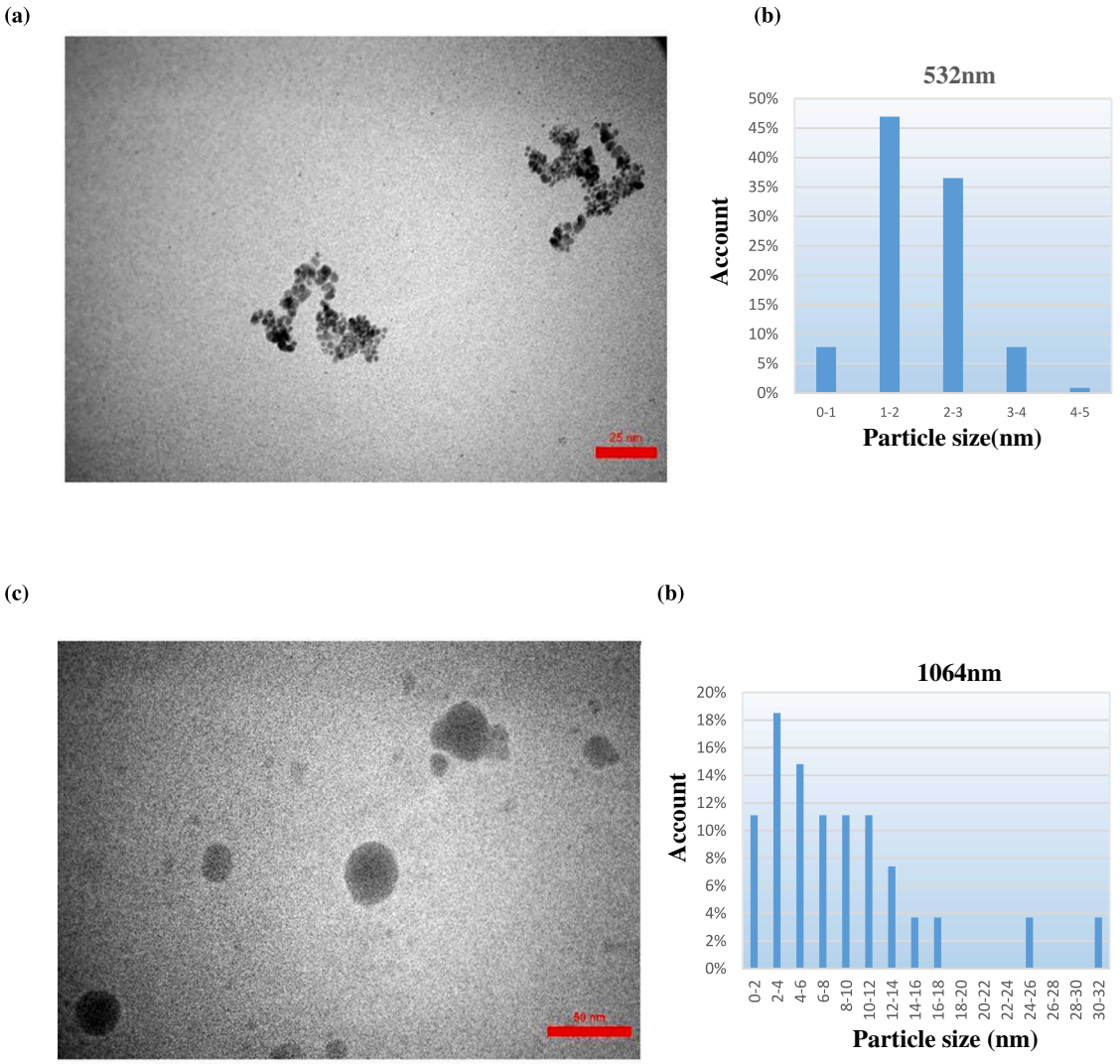

Fig. 4. TEM results of Gold nanoparticles at 12 Hz with two different laser fluencies and two laser ablation wavelengths: **(a)** F = 0.017 J/cm^2 and λ = 532 nm (Bar = 25 nm); **(b)** distribution diagram of Au nanoparticle for 0.017 J/cm^2 (N = 27, mean = 1.93 nm); **(c)** F = 0.028 J/cm^2 and λ = 1064 nm (Bar = 50 nm); **(d)** distribution diagram of Au nanoparticle for 0.028 J/cm^2 (N = 27, mean = 8.82 nm).

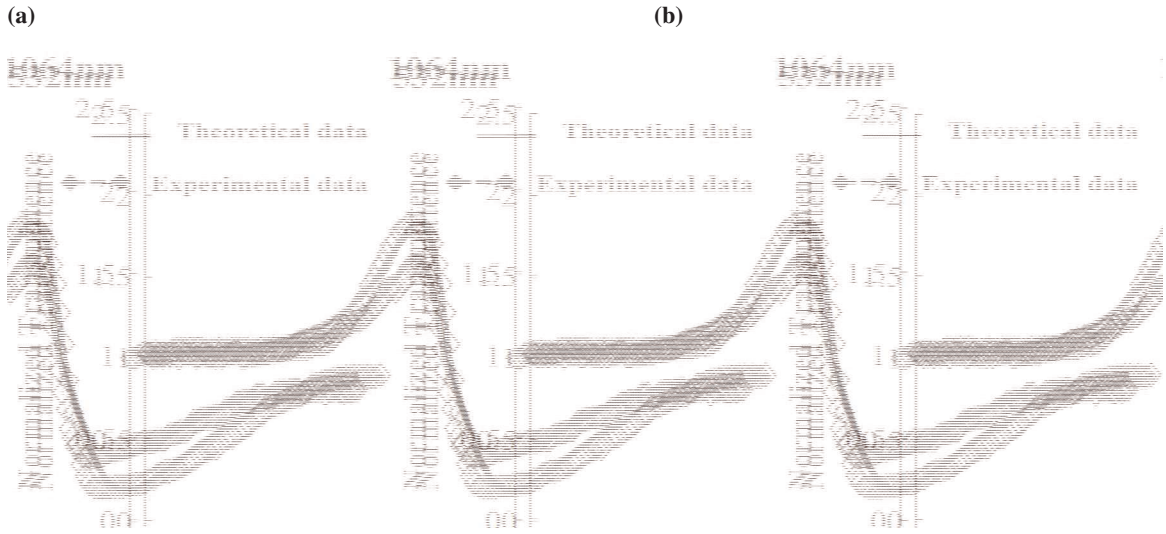

Fig. 5. Closed aperture Z-scan experimental data (dashed-diamond line) and theoretical curve (solid line) calculated using Eq. (4) for Ag NPs at 12 *Hz* in) **(a)** the laser radiation wavelength 532 nm and the laser fluency: 0.017 J/cm^2 **(b)** the laser radiation wavelength 1064 nm and the laser fluency: 0.028 J/cm^2.

$$\Delta T(z) = 1 - \frac{4\Delta\varphi_0 x}{(x^2+1)(x^2+9)}, \quad (4)$$

Where x is the normalized distance ($x = z/z_0$) and z_0 is the Rayleigh length. Nonlinear phase shift, $\Delta\varphi_0$, which is related to the nonlinear refractive index n_2, is (Sheik-Bahae et al., 1990):

$$n_2 = \frac{\Delta\varphi_0}{kL_{eff}I_0}, \quad (5)$$

Where $k = 2\pi/\lambda$ is the wave number, $L_{eff} = \frac{1-\exp(\alpha_0 L)}{\alpha_0}$ is the effective length of the nonlinear medium and L = 2 mm is the sample thickness at Z-scan.

Fig. 5(a) and (b) show the normalized transmittance,$\Delta T(z)$, for Au NPs produced at 12 *Hz* laser ablation repetition rate, two optimum fluencies: 0.017 J/cm^2 and 0.028 J/cm^2 and in two laser ablation wavelengths: 532 nm and 1064 nm, respectively.

The nonlinear phase shift,$\Delta\varphi_0$, gained after fitting Eq. (4) (solid line in Fig. 5) to the experimental data (dashed-diamond line in Fig. 5). The nonlinear refractive index of Au NPs in distilled water can be obtained from the Eq. (5). The existence of a peak before the focal point and a valley after the focal point in Fig. 5(a) and 5(b) demonstrate a negative nonlinear refractive index or self-defocusing effect. According to Fig. 3 (a), (b), the Au NPs consisted of substantial absorption around the $\lambda = 532nm$ (532 nm is the excitation laser wavelength in the Z-scan method).

Consequently, the observed nonlinearity effect in Fig. 5(a) and (b) may be due to the thermal effect. Since the amount of Sodium citrate is little in the water, we disregarded its effects on linear and nonlinear refractive and absorption coefficients.

Table 1 displays the amounts of $\alpha_0, n_2, \beta, |W|and|T|$ and the average size of Au NPs at 12 *Hz* pulse repetition rate for two optimum laser fluencies and two laser ablation wavelengths. According to the data from this table, the nonlinear refractive index increases as NP size increases. Moreover, According to Table 1, the nonlinear refractive index increases as the laser fluency and the size of NPs increase. This observation is because the nonlinear refractive index depends on the ratio of α/D(α is linear absorption coefficient, and D is thermal diffusivity). The ratio of (α/D) increased by increasing of the size of NPs (Shahriari and Moradi, 2015; Shahriari et al., 2010). On the other hand, the nonlinear refractive indices show larger values because of the small average size of NPs than those previously reported in articles (Sadrolhosseini et al., 2014; Shahriari et al., 2010).

The determined amounts of the two figures of merit $|w|$ and $|T|$ for Au NPs at 12 *Hz* pulse repetition rate for two optimum laser fluencies and two laser ablation wavelengths revealed that they are practical tools for all-optical switching devices.

3.2.2. Nonlinear absorption coefficient measurements (opened aperture Z-scan method)

To measure the nonlinear absorption coefficient at the Z-scan method, we have used the method of Ref. (Weber et al., 1978). The photodiode PD_2, is shown in Fig. 2, measures the irradiance, which depends on the absorption coefficient (β) in the open aperture. The dependence of absorption coefficient on laser radiation is given by (Jafari et al., 2018);

$$\alpha = \alpha_0 + \beta I, \quad (6)$$

For $\beta > 0$, we have a valley due to nonlinear two-photon absorption, and for $\beta < 0$, we have a peak due to nonlinear saturation absorption (Jafari et al., 2018). When the sample was moved along the z-axis and passed through the focal point of the lens, the irradiance of the laser increased at the cross-section of the beam, and the data were recorded by PD_2 that showed a valley (peak) at the position z = 0 for $\beta > 0 (\beta < 0)$.

All data were normalized to the transmittance of an open aperture when no samples were present. The normalized transmittance for the open aperture is given by (Sheik-Bahae et al., 1990):

$$T(z) = 1 - \frac{q_0}{2\sqrt{2}(1+x^2)}, \quad (7)$$

Where the nonlinear phase shift, q_0, is related to the nonlinear absorption coefficient β as,

$$q_0 = \beta I_0 L_{eff}, \quad (8)$$

Fig. 6(a) and (b) show the normalized transmittance,$T(z)$, for Au NPs produced at 12 *Hz* laser ablation repetition rate and two optimum laser fluencies: 0.017 J/cm^2 and 0.028 J/cm^2, in two laser ablation wavelengths: 532 nm and 1064 nm, respectively.

The nonlinear phase shift,$q_0(z)$, gained after fitting Eq. (7) (solid line in Fig. 6) to the experimental data (dashed-diamond line in Fig. 6). The nonlinear absorption coefficient of Au NPs in distilled water obtained from Eq. (8). According to Fig. 3(a), (b) (UV–visible spectrums), Au NPs showed substantial absorption around $\lambda = 532nm$. The existence of a valley in the nonlinear absorption in Fig. 6(a) and (b) indicates the existence of two-photon absorption. These nonlinear absorptions presumably arise from two-photon absorption.

Table 1 displays the amounts of $\alpha_0, n_2, \beta, |W|and|T|$ and the average size of Au NPs at 12 *Hz* pulse repetition rate for two optimum laser fluencies and two laser ablation wavelengths.

According to the data from this table, the nonlinear absorption coefficients decrease as the NP size and the laser fluency increase. The decrease in absorption coefficient with the increase in NP size is attributed to the large number of NPs that were accommodated in a volume if the particles become smaller (Jafari et al., 2018; Shahriari and Moradi, 2015).

On the other hand, the nonlinear absorption coefficients show larger values because of the small average size of NPs than those previously reported in articles (Sadrolhosseini et al., 2014; Shahriari et al., 2010).

If the size of metal NPs such as gold and silver is shorter than the Fermi electron wavelength, the energy bands become energy levels. As a result, an energy gap is created and the metal NP turns into a semiconductor NP.

The wavelength of the Fermi electron is the wavelength of the most energetic electron in the sea of free electrons of the metal NPs. It is generally around 1 nm. If this electron is also confined, the energy levels break down (Bera et al., 2010).

Fig. 7 shows the FTIR spectrum of nanoparticles/distilled water sample synthesized using the conditions of F = 0.028 J/cm^2,$\lambda = 1064nm$, f = 12 *Hz*, t = 5 min for Au NPs. This spectrum is a significant tool for the observation of functional groups, which are included the stabilization of synthesized metal NPs. The results of FTIR analysis expressed different peaks at 3431.14 cm^{-1}, 2958.53 cm^{-1}, 2922.81 cm^{-1}, 1744.73 cm^{-1}, 1628.06 cm^{-1}, 1459.52 cm^{-1}, 1255.55 cm^{-1}, 1167.02 cm^{-1}, 997.66 cm^{-1}, 973.27 cm^{-1}, 841.30 cm^{-1} that indicate the presence of capping/stabilization agent with Au NPs. A strong absorption band is observed between 3300 cm^{-1} and 3500 cm^{-1}, which can be assigned to the primary vibration mode of O—H stretching due to water molecules. In the result, the peak at the wave numbers.

3431.14 cm^{-1}, 2958.53 cm^{-1}, 2922.81 cm^{-1}, 1744.73 cm^{-1},

Table 1
The Amounts of $\alpha_0, n_2, \beta, |W|, |T|$ and average size of Au NPs for two optimum laser fluencies and two laser ablation wavelengths.

Pulse repetition rate (Hz)	Laser Fluency (J/cm^2)	Ablation Wavelength (nm)	α_0(1/cm)	n_2 (cm^2/GW)	β(cm/GW) × 10^5	Average Size of NPs (nm)	$\|W\|$	$\|T\|$
12	0.017	532	0.62	–17	2	1.93	4.2	0.6
12	0.028	1064	0.44	–22	1.03	8.82	7.7	0.02

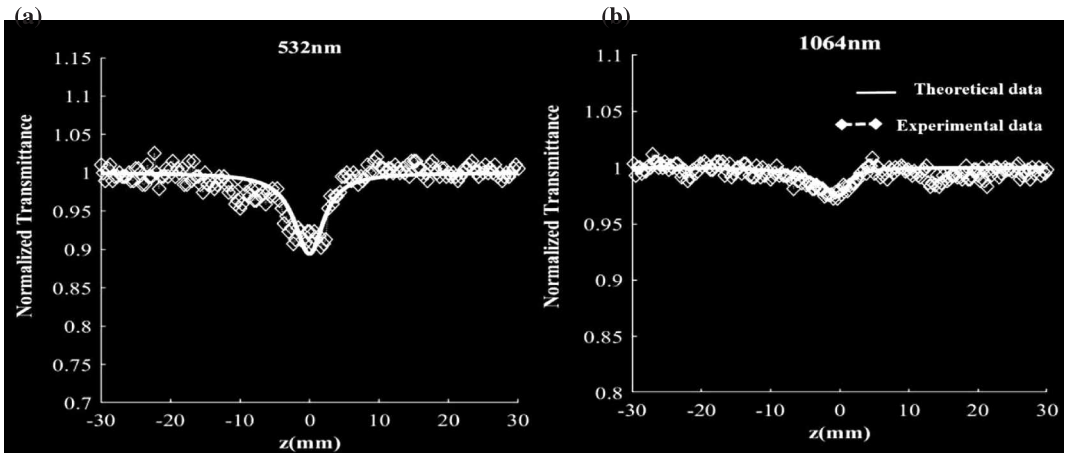

Fig. 6. opened aperture Z-scan experimental data (dashed-diamond line) and theoretical curve (solid line) calculated using Eq. (7) for Ag NPs at 12 *Hz* in **(a)** the laser radiation wavelength 532 nm and the laser fluency: 0.017 J/cm^2;**(b)** the laser radiation wavelength 1064 nm and the laser fluency: 0.028 J/cm^2.

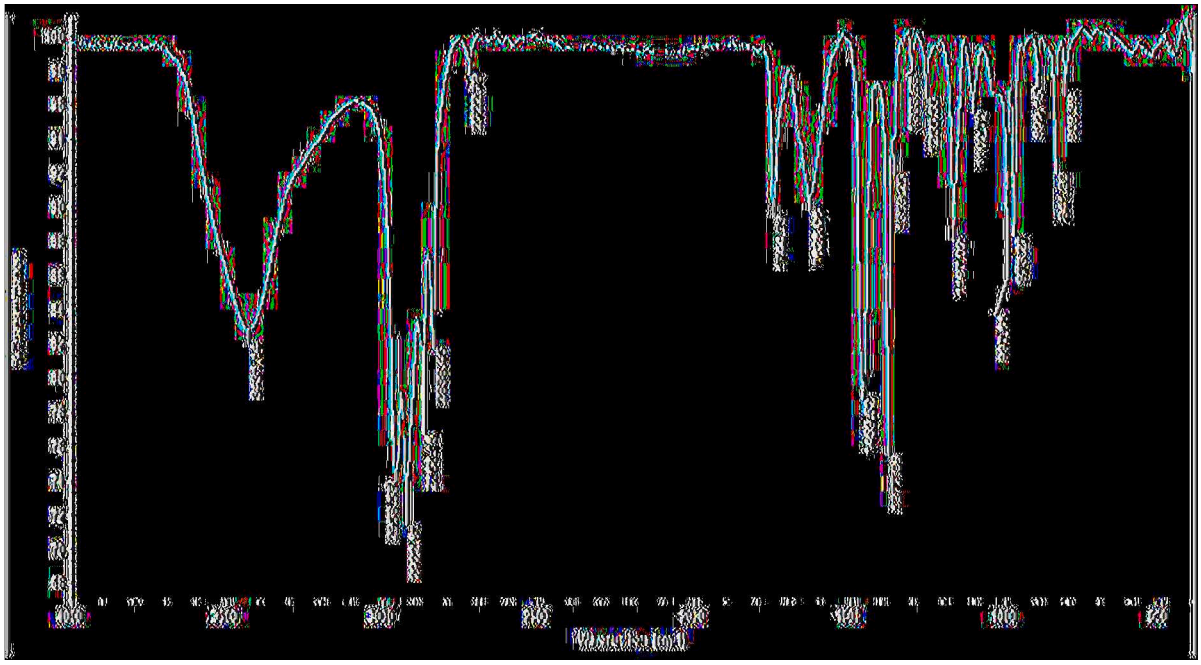

Fig. 7. FTIR spectrum of Au nanoparticles with Sodium citrate as stabilization for 12 *Hz* laser repetition rate and 0.028 J/cm^2 and $\lambda = 1064nm$ at 5 min.

1628.06 cm^{-1}can be assigned to the vibration of O—H stretching. The peaks at the wave numbers 1459.52 cm^{-1}, 1255.55 cm^{-1}and 1167.02 cm^{-1} can belong to C—C vibrations of covalent bonds and C—O stretching and C—O stretching, respectively.

The peaks at 997.66 cm^{-1} and 973.27 cm^{-1} correspond to the vibration bands of COOH and Au-NPs. This indicates that the Au NPs are tightly capped with COO^- and OH groups. The peak at 841.30 cm^{-1} are assigned to CH out of plane bending vibrations.

Then the solution is centrifuged at 10000 rpm for 15 min and washed three times. After drying, the resulting powder is prepared for XRD.

Fig. 8 shows the XRD spectrum of the sample synthesized using parameters: F = 0.028 J/cm^2,$\lambda = 1064nm$, f = 12 Hz, t = 5 min for Au NPs. According to the 96-900-8464 card, these peaks belong to the Fcc Au structure. The diffractograms show peaks located at $2\theta = 38.97°$, 45.37°, and 66.037° according to reflections of gold crystalline planes (1 1 1), (2 0 0) and (2 2 0), respectively. Table 2 shows the crystallite size for each peak using the Scherrer formula and the average size of Au NPs.

The obtained average size of Au NPs in TEM analysis is 8.82 nm

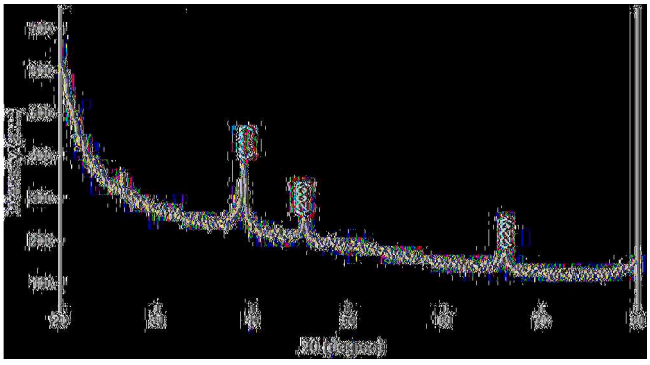

Fig. 8. XRD pattern of the sample was prepared for 12 *Hz* laser repetition rate and F = 0.028 J/cm^2, $\lambda = 1064nm$ at 5 min.

Table 2
The Amounts of 2[03*B*8], d spacing, diffraction peaks, crystal diameter, and the average size of Au NPs for laser fluency of F = 0.028 J/cm^2 and λ = 1064 nm.

Scherrer method			
2θ (deg.)	Inter planer distances (nm)	Diffraction peaks	Crystal diameter (nm)
38.97	0.231	(1 1 1)	12.4
45.37	0.199	(2 0 0)	14.9
66.037	0.141	(2 2 0)	5.9
average	–	–	11.06

(Fig. 4d), and the average size of Au NPs in the XRD study is 11.06 nm (Table 2). The size distribution of Au NPs extracted from TEM analysis is smaller than that determined from the XRD study, which shows the presence of NPs with a smaller diameter in the TEM image of Au NPs (Fig. 4c and 4d).

4. Conclusion

In conclusion, Au NPs were produced using Nd:YAG laser at two laser ablation wavelengths ($\lambda = 532nm$ and $\lambda = 1064nm$) and two optimum laser fluencies (0.017 J/cm^2 and 0.028 J/cm^2) at one pulse repetition rate. The Sodium citrate acts like a soft template and keeps the NPs apart and prevents the NPs from merging. As a result, the size of NPs becomes smaller. In addition, it used to control the size of NPs and capped Au^0 and Au^+ ions. In two different wavelengths, by adding a stabilizer and changing the laser fluency and laser pulse repetition rate, the best mode for producing gold nanoparticles with the smallest dimensions have been obtained. According to UV–Visible spectrum and TEM images, the surface Plasmon peaks for large Au NPs occurred at shorter wavelengths. The absorption peak height of the UV–Visible spectrum, as well as the distribution of Au NPs, increased when the laser ablation wavelength increased. The size of NPs can be controlled by increasing or decreasing the laser ablation fluency and the wavelength of laser radiation.

The obtained average diameters of NPs with the shape of spherical are 1.93 nm produced by laser ablation method at wavelength $\lambda = 532nm$ and 8.82 nm by laser ablation method at wavelength $\lambda = 1064nm$. The average size of NPs shows small values. Nonlinear refractive index and nonlinear absorption coefficient of Au NPs were investigated by Z-scan method. The results of the nonlinear refractive index show that the samples act as a strong concave lens, and the thermal self-defocusing effect can be the main factor of nonlinear behavior. The nonlinear refractive index increased when the laser ablation wavelength and the laser fluency increased. In addition, the nonlinear absorption coefficient decreased when the laser ablation wavelength and the laser fluency increased. Moreover, the nonlinear absorption coefficient exhibited a two-photon absorption behavior. As a result, the nonlinear absorption coefficients depend on the size of NPs and the laser ablation wavelength. The average size of NPs shows small values, consequently, the nonlinear refractive indices and nonlinear absorption coefficients indicate larger values than those previously reported in articles (it is 10^7 order of magnitude larger than what has been reported for the nonlinear refractive index in previous researches).

Finally, the Au NPs, which have been produced by laser ablation wavelength $\lambda = 1064nm$, and nonlinear refractive index ($-22\ \frac{cm^2}{GW}$), are used for chip-based sensors. According to the two figures of merit ($|W| \gg 1$ and $|T| \ll 1$), the Au NPs at the pulse repetition rate of 12 *Hz* for two laser ablation wavelengths are practical tools for all-optical switching devices. This is due to delocalized $\pi - electrons$ and the transforming of electron densities among the Au NPs and other substances.

Declaration of Competing Interest

The authors declare that they have no known competing financial interests or personal relationships that could have appeared to influence the work reported in this paper.

Data availability

Data will be made available on request.

Acknowledgements

We are deeply grateful to Urmia University for providing a fellowship for the present work.

References

Adair, R., Chase, L.L., Payne, A., 1987. Nonlinear refractive index measurement of glasses using three-wave frequency mixing. J. Opt. Soc. Anier. B 4, 875–881. https://doi.org/10.1364/JOSAB.455414.
Atile, A., Robinson, B.H., Seeman, N.C., 1987. The design of a biochip: A self-assembling molecular-scale memory device. Prot. Eng. 1, 295.
Bera, D., Qian, L., Tseg, T.K., 2010. Quantum Dots and their multimodel applications: a review. Materials (Basel) 3 (4), 2260–2345. https://doi.org/10.3390/ma3042.
Cai, W., Gao, T., Hong, H., Sun, J., 2008. Applications of gold nanoparticles in cancer nanotechnology. Nanotechnol. Sci. Appl. 1, 17–32. https://doi.org/10.2147/NSA.S3788.
Calderen-Jimenez, B., Montoro Bustos, A.R., 2022. Novel pathway for the sonochemical synthesis of silver nanoparticles with near-spherical shape and high stability in aqueous media. Nature, Sci. Rep. 12, 882. Doi: 10.1038%2Fs41598-022-04921-9.
Das, R., Babu, P.J., Gogoi, N., Sharma, P., Bora, U., 2012. Green Synthesis and Characterization of Biocompatible Gold Nanoparticles Using *Solanum Indicum* Fruits. J. ISRN Nanomaterials 2012, 1–6. https://doi.org/10.5772/56608.
De Góes, R.E., Muller, M., Fabris, J., 2017. Spectroscopic detection of glyphosate in water assisted by laser-ablated silver nanoparticles. Sensors 17 (5), 954. https://doi.org/10.3390/s17050954.
Fan, H.L., Ren, Q., Wang, X.Q., Sun, J., 2009. scrip. Nat. Sci. 1 (2), 136–141. https://doi.org/10.4236/ns.2009.12017.
Faraday, M., 1857. The Bakerian lecture: experimental relations of gold (and other metals) to light. Philos. Trans. Royal Soc. Lond. 147, 145–181. https://doi.org/10.1098/rstl.1857.0011.
Friberg, S.R., Smith, P.W., 1987. Nonlinear optical glasses for ultrafast optical switches. IEEE J. Quantum Electron QE-23, 2089–2094. https://doi.org/10.1109/JQE.1987.1073278.
Gentile, L., Mateos, H., Mallardi, A., Dell'Aglio, M., De Giacomo, A., Cioffi, N., Palazzo, G., 2021. Gold nanoparticles obtained by ns-pulsed laser ablation in liquids (ns-PLAL) are arranged in the form of fractal clusters. J. Nanopart. 23 (2) https://doi.org/10.1007/s11051-021-05140-5.
Góes, D., Possetti, R.E., Muller, G.R.C., 2020. IEEE. Sens. 20 (4), 1843–1850. https://doi.org/10.1109/JSEN.2019.2950161.
González-Castillo, J.R., Rodríguez-González, E., Jiménez-Villar, E., Cesar, C.L., Andrade-Arvizu, J.A., 2017. Assisted laser ablation: silver/gold nanostructures coated with silica, Springer. Appl. Nanosci. 7 (8), 597–605.
Hajiesmaeilbaigi, F., Mohammadalipour, A., Sabbaghzadeh, J., Hoseinkhani, S., Fallah, H.R., 2006. Preparation of silver nanoparticles by laser ablation and fragmentation in pure water. J. Phys. Lett. 3 (5), 252–256.
Huang, X., El-Sayed, M.A., 2010. Gold nanoparticles: optical properties and implementations in cancer diagnosis and photothermal therapy. Adv. Res. 1 (2010), 13–28. https://doi.org/10.1016/j.jare.2010.02.002.
Jafari, A., Zeynizadeh, B., Darvishi, S., 2018. Elsevier, Study of linear and nonlinear optical properties of nickel immobilized on acid-activated montmorillonite and copper ferrite nanocomposites. J. Mol. Liquid 253, 119–126. https://doi.org/10.1016/j.molliq.2018.010021.
Jiang, Z., Li, L., Huang, H., He, W., Ming, W., 2022. Progress in laser ablation and biological synthesis processes: "top-down" and "bottom-up" approaches for the green synthesis of Au/Ag nanoparticles. Int. J. Mol. Sci. 23 (23), 14658. https://doi.org/10.3390/ijms232314658.
Jiménez, I.O., Francisco, M.R., Neus, G.B., Puntes, V., 2010. Small Gold Nanoparticles Synthesized with Sodium Citrate and Heavy Water: Insights into the Reaction Mechanism. Physical Chem. C 114 (4), 1800–1804. https://doi.org/10.1021/jp9091305.
Koebel, M.M., Jones, C.L., Bowmaker, G.A., Nanopart, J., 2008. Research 10, 1063–1069. https://doi.org/10.1007/s11051-008-9370-7.
Kong, X.Y., Ding, Y., Yang, R., Wang, Z.L., 2004. Single-crystal nanorings formed by epitaxial self-coiling of polar nanobelts. Science 303, 1348–1351. https://doi.org/10.1126/science.1092356.
Maciulevičius, M., Vinčiūnas, A., Brikas, M., Butsen, A., Tarasenka, N., Tarasenko, N., Račiukaitis, G., 2013. On-line characterization of gold nanoparticles generated by laser ablation in liquids. J. Phys. Procedia 41, 531–538. https://doi.org/10.1016/j.phpro.2013.03.112.
Mashayekh, M., Dorranian, D., 2017. Third order optical nonlinearity of silver nanoparticles prepared by chemical reduction method. J. OptiK -Int. Light Electron Opt. 125, 5612–5618. https://doi.org/10.22401/JUNS.20.3.15.

MatIsa, S.Z., Zainon, R., 2022. State of the art in gold nanoparticle synthetization via pulsed laser ablation in liquid and its characterization for molecular imaging: a review. Materials 15, 875. https://doi.org/10.3390/ma15030875.

Nastulyavichus, A.A., Smirnov, N.A., Kudryashov, S.I., Ionin, A.A., Saraeva, I.N., Busleev, N.I., Rudenko, A.A., Khmel'nitskii, R.A., Zayarnyi, D.A., 2018. Formation of nanoparticles from thin silver films irradiated by laser pulses in air. Science 48 (3), 251–254. https://doi.org/10.1070/QEL16600.

Okitsu, K., Ashokkumar, M., Grieser, F., 2005. Sonochemical synthesis of gold nanoparticles: effects of ultrasound frequency. J. Phys. Chem. B 109 (44), 20673–20675. https://doi.org/10.1021/jp0549374.

Pyatenko, A., Shimokawa, K., Yamaguchi, M., Nishimura, O., Suzuki, M., 2004. Synthesis of silver nanoparticles by laser ablation in pure water. Appl. Phys. A: Mater. Sci. Process. 79, 803–806. https://doi.org/10.1007/s00339-004-2841-5.

Rad, A.G., Abbasi, H., Golyari, K., 2012. Fabrication and nonlinear refractive index measurement of colloidal silver nanoparticles. Appl. Phys. Math 2 (2), 135–139. https://doi.org/10.7763/IJAPM.2012.V2.69.

Sadrolhosseini, A.R., Noor, A.S.M., Faraji, N., Kharazmi, A., Mahdi, M.A., 2014. Optical nonlinear refractive index of laser-ablated gold nanoparticles graphene oxide composite. Nanomaterials 2014, 1–8. https://doi.org/10.1155/2014/962917.

Sadrolhosseini, A.R., Abdul Rashid, S., Zakaria, A., 2017. Synthesis of gold nanoparticles dispersed in palm oil using laser ablation technique. Nanomaterials 2017, 1–5. https://doi.org/10.1155/2017/6496390.

Saha, K., Agasti, S.S., Kim, C., Li, X., Rotello, V.M., 2012. Gold nanoparticles in chemical and biological sensing. Chem. Rev. 112 (5), 2739–2779. https://doi.org/10.1021/cr2001178.

Saitow, K., Okamoto, Y., Yano, Y.F., 2012. Size-selected submicron gold spheres: controlled assembly onto metal, carbon, and plastic substrates. J. Phys. Chem. C 116, 17252–17258. https://doi.org/10.1021/jp304109h.

Shahriari, E., Moradi, M., 2015. Investigation of nonlinear optical properties of Ag nanoparticles. IJOP 9 (2), 107–113.

Shahriari, E., Yunus, W., Saion, E., 2010. Effect of particle size on nonlinear refractive index of Au nanoparticle in PVA solution. Braz. J. Phys. 40 (2), 256–260. https://doi.org/10.1590/S0103-97332010000200021.

Sheik-Bahae, M., Said, A.A., Wei, T.-H., Hagan, D.J., Van Stryland, E.W., 1990. Sensitive measurement of optical nonlinearities using a single beam. IEEE J. Quantum Electron. 26 (4), 760–769. https://doi.org/10.1109/3.53394.

Sivakumar, P., Ramesh, R., Ramanand, A., 2011. Simple Co-precipitation synthesis and characterization of magnetic spinel $NiFe_2O_4$ nanoparticles. J. Mater. Lett. 65 (3), 483–485. https://doi.org/10.1016/j.matlet.2010.10.056.

Sortino, A.L., Censabella, M., Munzi, G., Boninelli, S., Privitera, V., Ruffino, F., 2020. Laser-based synthesis of au nanoparticles for optical sensing of glyphosate: a preliminary study. J. Micromachins 11 (11), 989. https://doi.org/10.3390/mi11110989.

Svedendahl, M., Chen, S.i., Dmitriev, A., Käll, M., 2009. Refractometric sensing using propagating versus localized surface plasmons: a direct comparison. Nano Lett. 9 (12), 4428–4433. https://doi.org/10.1021/nl902721z.

Tan, M.I.S., Omar, A.F., 2019. State of the art in gold nanoparticle synthetization via pulsed laser ablation in liquid and its characterization for molecular imaging: a review. Results Phys. 14, 102497 https://doi.org/10.1016/j.rinp.2019.102497.

Turkevich, J., Stevenson, P.C., Hillier, J., 1951. A study of the nucleation and growth processes in the synthesis of colloidal gold. Discussions Faraday Soc. 11, 55–75. https://doi.org/10.1039/DF9511100055.

Weber, M.J., Milam, D., Smith, W.L., 1978. Nonlinear refractive index of glasses and crystals. J. Opt. Eng. 17, 463–469. https://doi.org/10.1117/12.7972266.

Ying, Y., Rioux, R.M., Erdonmenz, C.K., HUghes, S., So-morjai, n.d.. Formation of nanoparticles from thin silver filmes irradiated by laser pulses in air.Science 304, 711. doi: 10.1070/QEL16600.